ACS Photonics

Open Access

pubs.acs.org/journal/apchd5

Article

Quantum Theory of Photon Pair Creation in Photonic Time Crystals

Jaime E. Sustaeta-Osuna,* Francisco J. García-Vidal, and P. A. Huidobro*

Cite This: ACS Photonics 2025, 12, 1873−1880

Read Online

ACCESS | Metrics & More | Article Recommendations | Supporting Information

ABSTRACT: Time-varying media offer a platform to realize novel and exotic wave effects, including photonic time crystals characterized by momentum band gaps with exponential wave amplification. Here we focus on the quantum electrodynamic properties of time-varying media, in particular, vacuum amplification and squeezing. For that purpose, we present a theory of photon pair generation in photonic time crystals that unveils the link between the classical and quantum electrodynamical properties of these systems: that is, a direct relation between reflectivity and pair generation through the squeezing parameter. By working within a Hermitian framework, we are able to characterize quantum pair generation processes in photonic time crystals, showing how momentum bandgaps result in an exponential enhancement of dynamical Casimir processes.

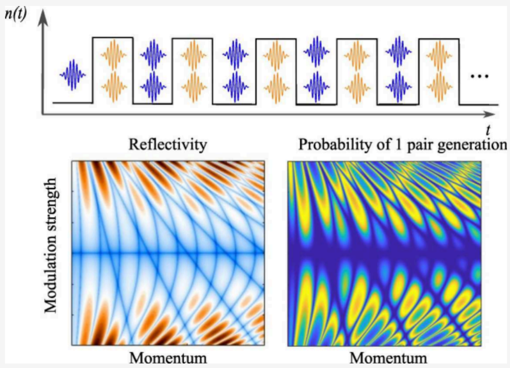

KEYWORDS: *time-varying media, photonic time crystals, transfer matrix, dynamical Casimir effect, squeezing*

■ INTRODUCTION

Time-varying media open new doors to controlling the propagation of electromagnetic waves.[1−4] When the optical parameters of a material are modulated in time, a myriad of new physical phenomena with no counterpart in spatially structured systems is unraveled. These include temporal refraction and reflection,[5] frequency conversion,[6−9] temporal diffraction,[10] a Fresnel light drag based on synthetic motion,[11] spatiotemporal metasurfaces,[12] or spontaneous emission from stationary charges,[13] among many others.[14−20]

The simplest example of a time-varying medium is a temporal interface, in which the material's optical properties change values instantaneously.[21−26] Such a system conserves momentum, but not frequency, and vertical transitions between different light cones take place.[27,28] Lack of energy conservation allows the incident (forward) wave to change frequency and be amplified, but for momentum to be the same before and after the switch, a backward wave emerges, also at a new frequency. These waves are manifestations of time refraction and reflection phenomena,[29,30] which have been observed for electromagnetic waves with transmission lines.[5]

Periodic temporal modulations result in a photonic time crystal (PTC), which displays band structures with momentum bandgaps where frequency is complex-valued.[4,27] PTCs have been experimentally realized in the microwave regime.[31,32] For their realization at higher frequencies, low Drude weight semiconductors, such as indium tin oxide (ITO), are promising candidates since they enable an ultrafast and unprecedentedly strong modulation of the refractive index.[33−39]

On the other hand, time varying media also offer a very rich platform from the point of view of quantum electrodynamical effects.[20,40−45] Through the interaction between quantum fluctuations and the dynamic properties of time-varying media, these systems allow the amplification of the quantum vacuum.[46] In particular, pairs of photons can be spontaneously created from the vacuum in a squeezed state at a temporal interface[41] through the dynamic Casimir effect.[46−49] Interestingly, time-varying media offer great control over vacuum amplification processes: anisotropic temporal boundaries provide angular control over vacuum amplification,[43] while quantum antireflection temporal coatings,[50] the temporal analogues of antireflection coatings, induce a frequency shift of the quantum state while preserving photon statistics.[44] Furthermore, synthetically moving gratings also result in radiation from the quantum vacuum in an analogue to Hawking radiation.[20] However, a complete theory of photon pair creation in PTCs that includes the bandgaps and the band edges within a fully analytic model is lacking, owing to the difficulty of dealing with the parametric instabilities that emerge in these time-periodic systems.[42,51−54]

In this work, we present a theory of photon pair creation in time-varying media in the PTC regime. For this purpose, we first consider the classical electrodynamics of PTCs and show

Received: November 19, 2024
Revised: March 10, 2025
Accepted: March 11, 2025
Published: April 2, 2025

https://doi.org/10.1021/acsphotonics.4c02293
ACS Photonics 2025, 12, 1873−1880

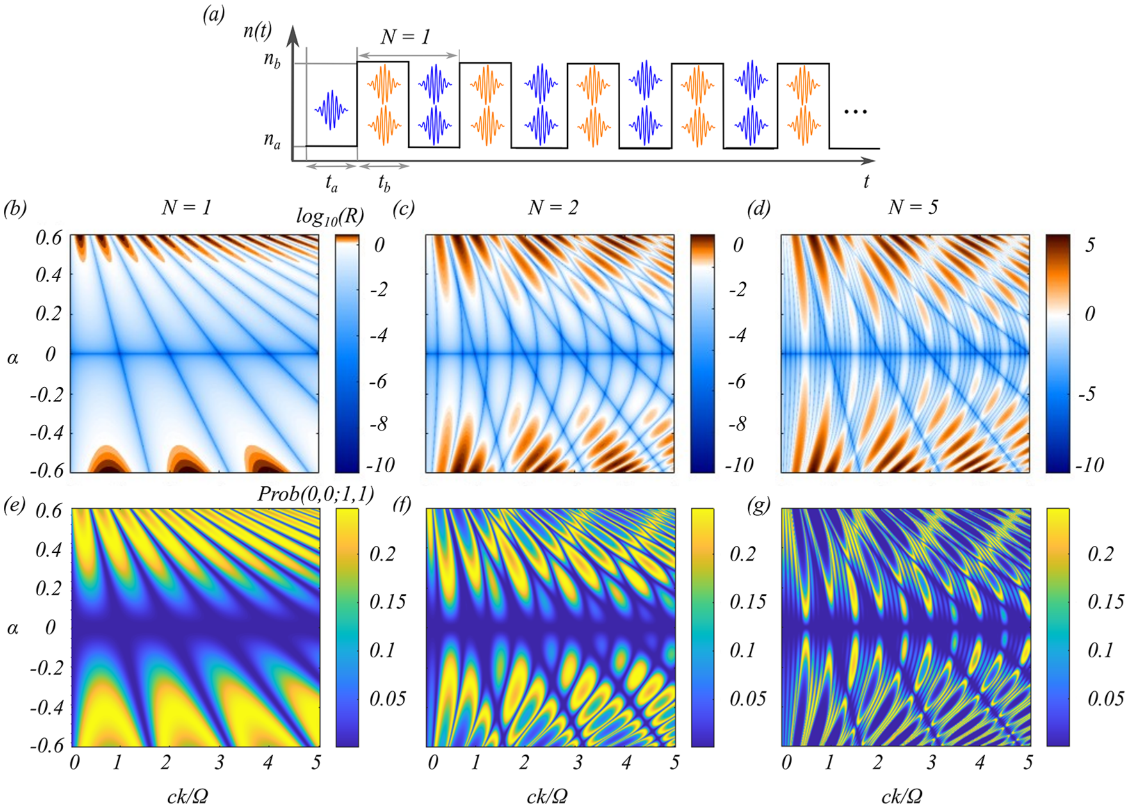

Figure 1. (a) Sketch of the PTC: the basic unit of the transfer matrix is a n_b slab, followed by a n_a slab. (b−d) Reflectivity, $\mathcal{R}$ (logarithmic scale) for $N = 1$ (b), $N = 2$ (c), and $N = 5$ (d) periods of the time modulation. (e−g) Probability for single photon pair creation from the vacuum, again for $N = 1$ (e), $N = 2$ (f), and $N = 5$ (g) periods.

that the physical properties that characterize this regime emerge when just a few temporal boundaries are considered. Next, we introduce field quantization through a transfer matrix approach. This allows us to describe photon pair generation within a Hermitian theory that is fully analytical and that includes the momentum bandgaps and the band edges. In doing so, we provide a direct link between the properties of classical light in PTCs, such as the reflectivity and quantum amplification effects. This way, we describe photon pair generation and squeezing in PTCs, showing how momentum bandgaps result in an exponential enhancement of dynamical Casimir processes.

■ METHODS

Let us consider a spatially homogeneous and isotropic medium whose permittivity, $\varepsilon(t)$, and thus refractive index $n(t)$, is periodically modulated in time, in a series of instantaneous temporal interfaces. The refractive index alternatively takes two values, n_a and n_b; we shall name each of these intervals with a constant refractive index a *temporal slab* or *slab* for abbreviation. Each slab with $n(t) = n_a$ lasts for a time t_a, while those with $n(t) = n_b$ do so for a time t_b, with $T = t_a + t_b$ being the period of the PTC. Such a system is depicted in Figure 1a. Since the medium is homogeneous and isotropic, both the wavevector $\boldsymbol{k}$ and the polarization σ are conserved quantities; however, as commented above, the frequency is not, and vertical transitions take place between the light cones of adjacent slabs.[27] Applying temporal boundary conditions to Maxwell equations (see Supporting Information for details), we build up a transfer matrix and use it to connect the field amplitudes of different $n(t) = n_a$ temporal slabs,[13] as

$$\begin{pmatrix} (B^{(N)}_{-\boldsymbol{k}\sigma})^* \\ B^{(N)}_{\boldsymbol{k}\sigma} \end{pmatrix} = \boldsymbol{T}^N \cdot \begin{pmatrix} (B^{(0)}_{-\boldsymbol{k}\sigma})^* \\ B^{(0)}_{\boldsymbol{k}\sigma} \end{pmatrix} \tag{1}$$

Here, $B^{(N)}_{\boldsymbol{k}\sigma}$ is the amplitude of the magnetic induction flux within the Nth n_a-type slab, with wavevector $\boldsymbol{k}$ and polarization σ, and $\boldsymbol{T}$ is the transfer matrix. The $\boldsymbol{T}$-matrix couples forward ($\boldsymbol{k}$) and backward modes ($-\boldsymbol{k}$) at the 0th and Nth slabs and guarantees that momentum is conserved. The transfer matrix depends on the polarization σ of the mode only through a change of sign in the off-diagonal elements of $\boldsymbol{T}^N$, which shall be of no importance when calculating classical amplification and photon pair creation (see SI). Therefore, and taking also into account that the $\boldsymbol{T}$-matrix does not couple modes with different polarizations, we shall omit the σ subscript from now on.

The eigenvalues $\lambda_\pm$ of the $\boldsymbol{T}$-matrix are given by

$$\lambda_\pm = p \mp \mathrm{i}\sqrt{1 - p^2},$$

where

$$p = \cos\left(\frac{ckt_a}{n_a}\right)\cos\left(\frac{ckt_b}{n_b}\right) - \frac{n_a^2 + n_b^2}{2n_a n_b}\sin\left(\frac{ckt_a}{n_a}\right)\sin\left(\frac{ckt_b}{n_b}\right).$$

The parameter p, which depends on the wavenumber k, controls whether the eigenvalues form complex conjugate pairs with unit modulus, which happens for $|p| < 1$, or if they are real-valued, which occurs when $|p| > 1$. Lastly, for the $|p| = 1$ case, the two eigenvalues become degenerate and we have an exceptional point.[55] On the other hand, from their definition we see that $\lambda_+\lambda_- = 1$. This enables us to introduce a Floquet

https://doi.org/10.1021/acsphotonics.4c02293
ACS Photonics 2025, 12, 1873−1880

frequency, ω_F through $\lambda_\pm = \exp(\mp i\omega_F T)$. From our previous analysis we see that for $|p| < 1$ the Floquet frequencies are real-valued, while for $|p| > 1$ they are complex. These k intervals with complex ω_F define the momentum bandgaps of the PTC, in which exponential amplification of electromagnetic waves takes place and that can be populated due to energy not being conserved in these systems.[56] As we will see, the $\boldsymbol{T}$-matrix enables us to study the emergence of the PTC regime as more layers are added to the system.

From the realness of the solutions to Maxwell equations, as well as the conservation of momentum, we can infer the following properties of the transfer matrix (see SI): $(\boldsymbol{T}^N)_{11} = ((\boldsymbol{T}^N)_{22})^*$ and $(\boldsymbol{T}^N)_{12} = ((\boldsymbol{T}^N)_{21})^*$, as well as $\det(\boldsymbol{T}) = 1$. These properties enable us to write

$$(\boldsymbol{T}^N)_{11} = \cosh(r)e^{i\theta_1} \tag{2}$$

$$(\boldsymbol{T}^N)_{12} = \sinh(r)e^{i\theta_2} \tag{3}$$

where θ_1 and θ_2 are, respectively, the phases of forward and backscattered waves, and r measures the strength of forward amplification and backscattering. It can also be proved (see SI) that

$$(\boldsymbol{T}^N)_{12} = \frac{\sin(N\omega_F T)}{\sin(\omega_F T)}(\boldsymbol{T})_{12} \tag{4}$$

Importantly, eq 4 only assumes the modulation to be periodic, with its shape otherwise completely arbitrary. The particular modulation profile chosen (either a step or something smooth) determines only the dispersion relation for ω_F. Here we study the step as a proof of concept, since in this case an analytical formula for ω_F can be derived, as seen above. Furthermore, the classical transmitivity and reflectivity of the PTC are given by $\mathcal{T} = |(\boldsymbol{T}^N)_{11}|^2 = \cosh^2(r)$ and $\mathcal{R} = |(\boldsymbol{T}^N)_{12}|^2 = \sinh^2(r)$, respectively. As a consequence of momentum conservation, $\mathcal{T} - \mathcal{R} = 1$. From this constraint we see $\mathcal{T} \geq 1$, meaning the temporal modulation can only enhance (or be transparent to) an incoming signal, but never suppress it, and always at the expense of some backscattering.

Both the transmitivity and reflectivity depend on the wavenumber k, the two values taken by the refractive index n_a and n_b, the duration of each slab t_a and t_b, and last, the number of modulation periods, N. For the sake of simplicity, we assume $t_a = t_b$, and $n_a = 1 + \alpha$ and $n_b = 1 - \alpha$, with $-1 < \alpha < 1$ measuring the strength of the modulation.

■ RESULTS

Making use of the $\boldsymbol{T}$-matrix method described above, we first study the classical reflectivity of the PTC as more slabs/periods are added to it. In Figure 1b−d we show the reflectivity for N = 1, 2, and 5 slabs as a function of both α and ck/Ω, where c is the speed of light in the unmodulated medium ($\alpha = 0$) and $\Omega = 2\pi/T$ is the modulation frequency. The orange regions correspond to a reflectivity larger than unity and, hence, to a strong backscattering, while the blue ones exhibit a comparatively weaker temporal reflection. For $N = 1$, see panel (b), high backscattering regions appear for large values of $|\alpha|$. However, these orange regions progressively tend toward the $\alpha = 0$ horizontal line (in which $\mathcal{R} = 0$) as the number of periods of the PTC increases [see panels (c) and (d) in Figure 1]. Hence, wave amplification can be achieved with a weaker modulation if it is sustained for a longer time. As we will see, this is related to the emergence of the PTC regime.

On the other hand, for $N = 1$ (Figure 1b), we see dark blue lines with a negative slope in which the reflectivity vanishes: these are the transparency lines of the temporal slab, which satisfy $(\boldsymbol{T})_{12} = 0$, the antireflection temporal coating condition,[15,44,50] and come from destructive interference between waves backscattered at $t = t_a$ and $t = t_a + T$. As the number of periods of the PTC increases, new transparency lines start emerging, as seen in Figure 1c,d. These are the zeros of $(\boldsymbol{T}^N)_{12}$ (eq 4), which also come from the destructive interference of waves backscattered at different time interfaces. As seen in both panels, the more slabs added to the PTC, the more transparency lines accumulate, as can also be inferred from the N-dependence of the formula for $(\boldsymbol{T}^N)_{12}$. We also see how the figures become more symmetric with respect to the $\alpha = 0$ horizontal line as N increases; this is expected, since after modulating for a sufficiently long time, the initial value of ε (either n_a^2 or n_b^2) becomes unimportant (unless the mode happens to satisfy $(\boldsymbol{T})_{12} = 0$).

Thus, from our approach we can draw conclusions about the emergence of the PTC regime with just a few temporal slabs, $N \geq 2$. While some broad ranges of values of momentum entail an exponential amplification of modes (orange areas in Figure 1c,d), the number of transparency lines, in which destructive interference eliminates any previous amplification, increases with N (dark blue areas in the plots). The first phenomenology corresponds to the momentum band gaps, and the second corresponds to the bands, as we will see more clearly below.

Next, we quantize the field within each temporal slab (see SI). Employing canonical quantization, the photon operators of different slabs can be shown to be connected through the same transfer matrix as the classical fields. This connection results in a Bogoliubov transformation of the operators along the PTC,[41,43,44]

$$(\hat{a}_{-\boldsymbol{k}}^{(N)})^\dagger = \cosh(r)e^{i\theta_1}(\hat{a}_{-\boldsymbol{k}}^{(0)})^\dagger + \sinh(r)e^{i\theta_2}\hat{a}_{\boldsymbol{k}}^{(0)} \tag{5}$$

$$\hat{a}_{\boldsymbol{k}}^{(N)} = \cosh(r)e^{-i\theta_1}\hat{a}_{\boldsymbol{k}}^{(0)} + \sinh(r)e^{-i\theta_2}(\hat{a}_{-\boldsymbol{k}}^{(0)})^\dagger \tag{6}$$

where $\hat{a}_{\boldsymbol{k}}^{(N)}$ annihilates a photon with wavevector $\boldsymbol{k}$ for $t \in [NT, NT + t_a)$, and correspondingly for the creation operators. The parameters r and $\theta_{1,2}$ come from the classical transfer matrix, see eqs 2 and 3. On the other hand, and as can be seen from eqs 5 and 6, such transformation between forward and backward photon operators implement a squeezing operation.[57−59] Thus, by defining the complex squeezing parameter

$$\zeta = r\exp(i\varphi) \tag{7}$$

where we recall that r gives the classical reflectivity, $\mathcal{R} = \sinh^2(r)$ and where $\varphi = \theta_1 - \theta_2$, we can introduce the following two-mode squeezing operator

$$\hat{S}(\zeta) = \exp(\zeta\hat{a}_{\boldsymbol{k}}^{(0)}\hat{a}_{-\boldsymbol{k}}^{(0)} - \zeta^*(\hat{a}_{\boldsymbol{k}}^{(0)})^\dagger(\hat{a}_{-\boldsymbol{k}}^{(0)})^\dagger) \tag{8}$$

which acts as the unitary time-evolution operator in this theory (SI). Thus, we see how each time interface results in the generation of photon pairs, with forward and backward photons being correlated in a squeezed state owing to momentum conservation.[41,43,44]

Critically, our transfer matrix approach enables a full analytical study of the quantum electrodynamics of the whole band structure, including the bandgaps and the band edges. This is in contrast to previous quantum mechanical descriptions of PTCs, which have so far either neglected the bandgaps and band edges or dealt with them numerically with FDTD methods,[42] owing to the difficulty of including them within a Hermitian theory.[54,55]

With our framework, we can compute photon transition probabilities. These can be obtained from the matrix elements of the squeezing operator in the number state basis,

$$\langle n_{\boldsymbol{k}}',\, m_{-\boldsymbol{k}}'|\hat{S}(\zeta)|n_{\boldsymbol{k}},\, m_{-\boldsymbol{k}}\rangle = \frac{(-e^{i\varphi}\tanh(r))^{n'-n}}{(\cosh(r))^{n+m+1}} \sum_{l=\max(0,n-n')}^{\min(n,m)} C^{l}_{n,m;n',m'}(-\sinh^2(r))^{l}\delta_{n'-n,m'-m}, \tag{9}$$

where

$$C^{l}_{n,m;n',m'} = \frac{\sqrt{n'!m'!n!m!}}{l!(l+n'-n)!(n-l)!(m-l)!} \tag{10}$$

and where the Kronecker delta in eq 9 ensures momentum conservation. The probability for the transition $|n_k, m_{-k}\rangle \to |n_k', m_{-k}'\rangle$ is then given by $\mathrm{Prob}(m,n;n',m') = |\langle n_k',m_{-k}'|\hat{S}(\zeta)|n_k,m_{-k}\rangle|^2$. Also, as was the case for the transfer matrix formulas, eq 9 applies to any periodic modulation, with details of the modulation entering through the dispersion relation and the squeezing parameter.

In Figure 1e−g, we plot the probability of creating a single photon pair starting from the vacuum state, i.e., $|\langle 1_k 1_{-k}|\hat{S}(\zeta)|0_k,0_{-k}\rangle|^2$, for the same values of N, as considered in Figure 1c,d. For the case of a single temporal slab, $N = 1$, a correspondence between the classical reflectivity of the PTC, $\mathcal{R} = \sinh^2(r)$, and the quantum transition probabilities between number states can be inferred by comparing Figure 1b and e. As may be expected intuitively, we find a connection between strong backscattering and high photon pair creation probabilities, while weak backscattering implies low photon pair creation probabilities. However, for $N = 2$ this correspondence between the classical and quantum quantities starts to disappear. In particular, the regions of largest reflectivity and sufficient large $|\alpha|$ in Figure 1c do not correspond to regions of the largest photon pair creation probability, Figure 1f, but to regions of a very low one. Results for a larger number of slabs ($N = 5$) show that this effect is even more pronounced (compare Figure 1d and g), and the (yellow) pockets of high pair creation probability become smaller and migrate toward lower values of $|\alpha|$. Since our theory is unitary, there cannot be a probability leakage to a surrounding environment; as we will show below, what is happening is that the probability, which is conserved, is migrating toward higher order processes $|0_k, 0_{-k}\rangle \to |m_k, m_{-k}\rangle$, for $m > 1$, thus reducing the probability of creating a single pair ($m = 1$). Interestingly, the photon pair creation probability in PTCs is quite broad in the photon free-space frequency ck/Ω. This can be understood from the fact that in time-varying media energy is not conserved and that, contrary to the optical parametric amplifier,[60,61] there is no frequency matching to be made between the pump and the amplified waves.

We now study in detail the dependence of the photon transition probabilities on the number of photon pairs created. Figure 2 shows, for a fixed value of $\alpha = 0.5$ and for an increasing number of PTC periods ($N = 1$, 2, 3, 4, and 5), the reflectivity (a) and the transition probabilities for $m = 0$, 1, 2, and 3 pairs (b). In the lower-most panel of each column, we plot the dispersion relation of the PTC, from the Floquet frequencies obtained from the $\boldsymbol{T}$-matrix. We plot $\mathrm{Re}(\omega_F)$ in blue and $\mathrm{Im}(\omega_F)$ in orange so that the momentum band gaps can be clearly identified. By looking at the reflectivity plots as N increases (a) and considering the PTC dispersion relation, it is clear that the reflectivity exponentially increases with the number of slabs within the momentum bandgaps for values of N as low as 2 or 3. The nonvanishing imaginary part of the Floquet frequency is responsible for this and results in larger amplification for k values around $\sim 0.75\Omega/c$ due to the larger value of $\mathrm{Im}(\omega_F)$ in this gap than in the other two shown in the figure. Conversely, within the bands, the reflectivity stays lower and the addition of transparency lines where $\mathcal{R} \to 0$ as N increases can be clearly seen.

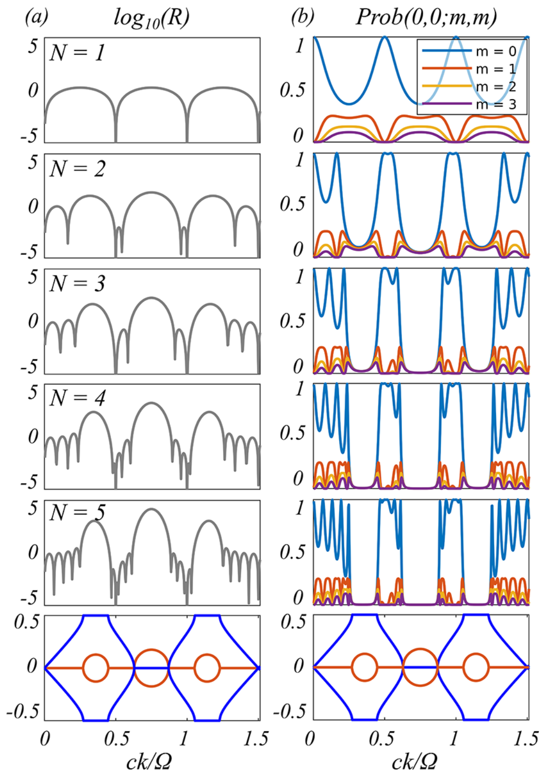

Figure 2. Evolution of PTC classical (a) and quantum (b) properties with a number of temporal slabs for a fixed modulation strength ($\alpha = 0.5$). (a) Reflectivity, $\mathcal{R}$, is shown in the top 5 panels ($N = 1$, 2, 3, 4, and 5, from top to bottom; saturation has been set to −5). (b) The m-pair ($m = 0$, 1, 2, and 3) photon pair creation probability starting from the vacuum state is shown in the top panels, corresponding to $N = 1$, 2, 3, 4, and 5 slabs, as in panel (a). In both columns, the lowermost panels show the Floquet frequency versus the wavevector (first Brillouin zone), with the real part of ω_F in blue and the imaginary part in orange.

Figure 2b shows photon transition probabilities from the vacuum state calculated with eqs 9 and 10. For all values of N, we see that the photon pair creation probability behaves very differently depending on whether k belongs to a band or a gap (see the bottom panel for the dispersion relation). Let us first focus on values of momentum that lie within the band of the PTC: it is clear that, independent of N, and for a fixed k, photon transition probabilities decrease as m increases. However, the particular shape of the probability curves greatly depends on N, with all the lines displaying more oscillations as the number of slabs increases, related to the behavior of the reflectivity in Figure 2a. In particular, there are a series of k

https://doi.org/10.1021/acsphotonics.4c02293
ACS Photonics 2025, 12, 1873−1880

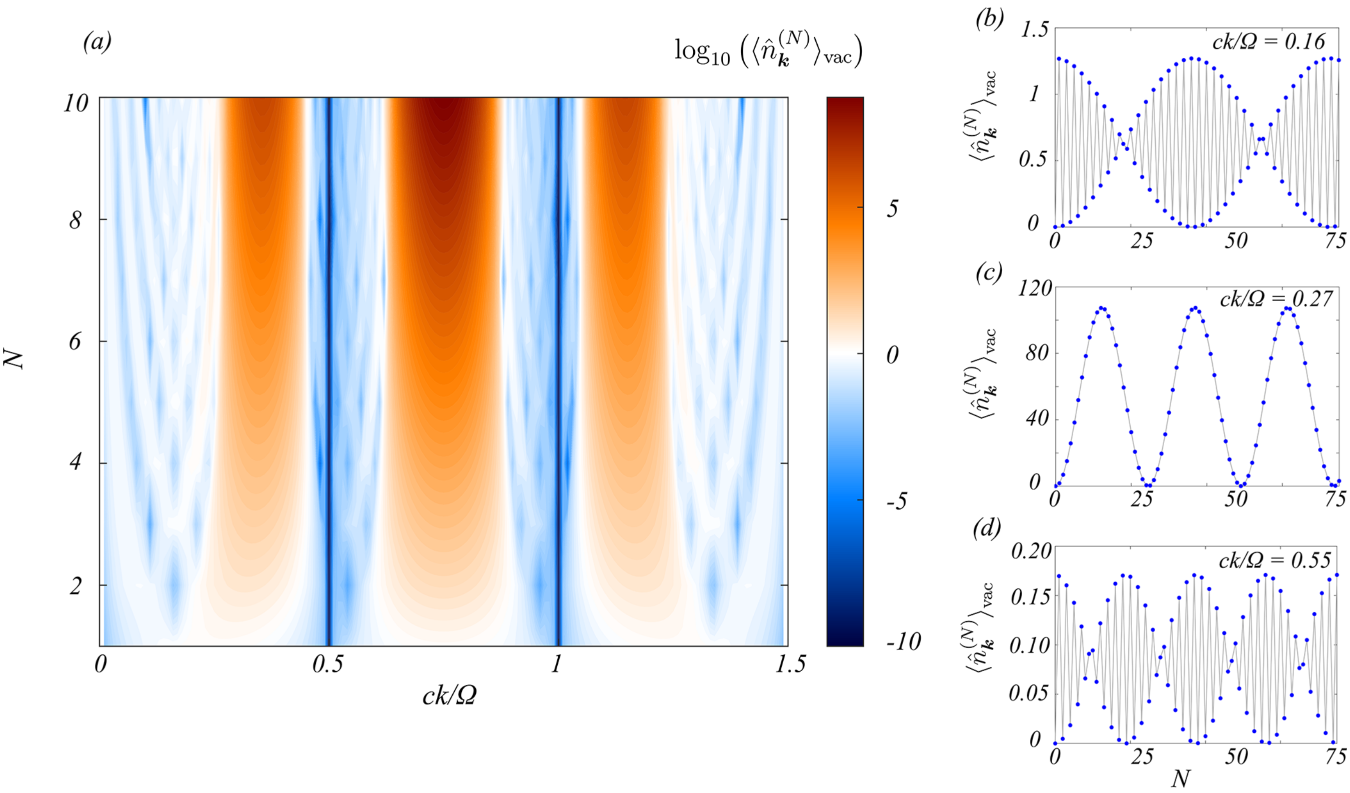

Figure 3. (a) Evolution of the average photon number extracted from the vacuum, $\langle \hat{n}_k^{(N)} \rangle_{\mathrm{vac}}$, with the number of periods of the time modulation, N. The modulation strength is $\alpha = 0.5$, and the saturation has been set to the lowest value -10 for a better visualization. In the right panels we plot $\langle \hat{n}_k^{(N)} \rangle_{\mathrm{vac}}$ for $ck/\Omega = 0.16$ (b), 0.27 (c), 0.55 (d). All three values lie within the bands: the first two belong to the leftmost one, while the third one belongs to the second band starting from the left.

values where the probability of no transition ($m = 0$) is maximum (equal to unity), while all of the other transitions ($m \geq 1$) are zero. These points originate from the transparency conditions of the PTC, where $(\boldsymbol{T}^N)_{12} = 0$. In between these points, all the photon pair creation probabilities show maxima, with the single pair case ($m = 1$) reaching a value of up to ~0.25. However, as we have discussed, the number of transparency lines increases with N; therefore, sustaining the periodic modulation for a longer time makes the PTC transparent to more waves. Thus, it is not always optimal to have long lasting modulations in order to maximize the probability of photon pair creation for a momentum value within the band, since any mode with real Floquet frequency will eventually pass through the modulation unperturbed for some value of N and periodically thereafter (with the period itself being k-dependent). Moreover, since the separation between transparent modes (those satisfying $(\boldsymbol{T}^N)_{12} = 0$) goes like $\Delta\omega_{\mathrm{F}} \sim 1/N$ (SI), in the $N \gg 1$ limit we have $\Delta\omega_{\mathrm{F}} \to 0$. Therefore, in the deep photonic time crystal regime, the separation between any two consecutive modes transparent to the time modulation vanishes, with the latter becoming transparent to all band modes in the $N \gg 1$ limit.

Now, focusing on the bandgaps, we see that all the probabilities get progressively squashed toward zero as N increases and become vanishingly small, with seemingly no photons being created inside the momentum gaps, for $N \geq 3$. However, such a conclusion would ignore that higher order transitions ($m \geq 4$) take place and become more probable as the squeezing strengthens (for complex ω_{F}, $r \sim N$ for $N \gg 1$), with lower order transitions necessarily becoming less probable. Furthermore, for a given squeezing strength, r, we have that $\mathrm{Prob}(0{,}0;m{,}m) = (\tanh^m(r)/\cosh^{m+1}(r))^2$, which enables us to write

$$\mathrm{Prob}(0,\ 0;\ \mathrm{m},\ \mathrm{m}) = \frac{\mathcal{R}^m}{(1+\mathcal{R})^{m+1}} \tag{11}$$

which decays monotonously with m for fixed $\mathcal{R}$. Also, $\mathrm{Prob}(0{,}0;m{,}m) \to 0$ as $\mathcal{R} \to \infty$, such as within the band gaps, for any value of m (a more in-depth discussion is found in the SI). Therefore, the m-photon pair creation probability becomes more and more uniform within the bandgaps as more periods are added to the PTC and the generation of pairs of photons becomes asymptotically uniform with m in the $N \gg 1$ limit. Hence, the photon number becomes, on average, very large, with all transitions between number states being equally probable, and although photons are indeed created, there is uncertainty on how many. Finally, we note that in Figures 1 and 2 we focus on values of the number of slabs of up to $N = 5$, as we find that these values, although similarly low, already display all the phenomenology of PTCs. Results for larger values of N are shown in the SI. The quantum statistics of the modes are also discussed in the SI, following refs 62−64.

So far, we have studied the classical and quantum amplification that occurs in these time-periodic systems and discussed the connection between them. We now make such a connection completely explicit by showing that the average photon number extracted from the vacuum actually coincides with the classical reflectivity of the PTC. For that purpose, we calculate the mean photon number at slab N, $\langle \hat{n}_k^{(N)} \rangle_{\mathrm{vac}} = \langle (\hat{a}_k^{(N)})^\dagger \hat{a}_k^{(N)} \rangle_{\mathrm{vac}}$, through the Bogoliubov transformations given by eqs 5 and (6). The expectation value is calculated in the

https://doi.org/10.1021/acsphotonics.4c02293
ACS Photonics 2025, 12, 1873−1880

vacuum state annihilated by the initial field operators (i.e., $\hat{a}_k^{(0)}|\text{vac}\rangle = 0$). This procedure for computing expectation values is the one employed in the Heisenberg picture, in which only the operators evolve in time, while the wave function remains unchanged with respect to its initial condition. Proceeding like this, we arrive to $\langle \hat{n}_{\boldsymbol{k}}^{(N)} \rangle_{\text{vac}} = \sinh^2(r) = \mathcal{R}$. Thus, we show that the classical reflectivity coincides with the mean number of photon pairs generated through quantum vacuum amplification. We once again emphasize that this result is independent of the chosen modulation profile as long as it is periodic in time.

In Figure 3a we plot $\langle \hat{n}_k^{(N)} \rangle_{\text{vac}} = \mathcal{R}$ for different values of the wavenumber, for a varying number of periods N between 1 and 10, and for a fixed value of $\alpha = 0.5$. The orange regions of the contour plot correspond to the momentum bandgaps of the band structure, while the white to blue ones are the band modes with real Floquet frequency. In the band gap, quantum vacuum amplification is much stronger, and the number of photons grows exponentially with the number of periods N. This can be seen explicitly from the analytical expression for $(\boldsymbol{T}^N)_{12}$ given by eq 4. By assuming complex-valued ω_{F} in the latter and taking the limit $N \gg 1$, we arrive at the asymptotic expression $(\boldsymbol{T}^N)_{12} \sim \exp(N\ \text{Im}(\omega_{\text{F}})T)$. Upon squaring its absolute value, we find $\langle \hat{n}_k^{(N)} \rangle_{\text{vac}} \sim \exp(2N\ \text{Im}(\omega_{\text{F}})T)$ and see that, indeed, there is exponential growth in the mean photon number inside the momentum gaps. Our previous analysis assumes $\text{Im}(\omega_{\text{F}})$ is positive, but this is not a problem: since the sine function in eq 4 becomes a hyperbolic sine for the case of complex ω_{F}, both $\text{Im}(\omega_{\text{F}}) > 0$ and $\text{Im}(\omega_{\text{F}}) < 0$ are accounted for. Thus, in the $N \gg 1$ limit, the $\text{Im}(\omega_{\text{F}}) > 0$ term dominates and is the one to appear in the asymptotic formula discussed above.

On the other hand, a glance at the white to blue colored areas in Figure 3a shows that the phenomenology is different for modes within the band in which the mean photon number is much smaller. From a classical point of view, this has to do with the fact that waves within the bands do not interfere constructively enough after being scattered by the temporal interfaces, resulting in a classical reflectivity $\mathcal{R}$ and hence, in a mean photon number $\langle \hat{n}_k^{(N)} \rangle_{\text{vac}}$, that remains bounded with N (see eq 4). Additionally, the magnitude of the average photon number is larger by at least 1 order of magnitude in the first (fundamental) and fourth bands than in the second and third ones. Looking at the band structure presented in Figure 2, we see that in these second and third bands dispersion is much stronger and the (k,ω_{F}) curve deviates more from the linear free space one, owing to the influence of the neighboring momentum gaps. This suggests that, in the scenario in which ω_{F} is real-valued, a matching between k and ω_{F} (except for a multiplicative constant with dimensions of velocity) favors vacuum quantum amplification. This is better seen in Figure 3b−d, in which we plot $\langle \hat{n}_k^{(N)} \rangle_{\text{vac}}$ for $ck/\Omega = 0.16$, 0.27, and 0.55, respectively. The first two values of momentum lie within the first (fundamental) band (b,c) while the third one belongs to the second band (c). We see that the photon number oscillates with N and that, for $ck/\Omega = 0.16$ (b) and 0.55 (d), it exhibits a periodic frequency beat. This beating is rooted in the competition between constructive and destructive interference between waves backscattered at different temporal interfaces, and it begins to disappear as we approach the momentum bandgap, as can be seen in Figure 3c. This can be understood from the fact that in the bandgaps constructive interference dominates and classical waves and vacuum quantum amplification become exponentially amplified. Mathematically, this frequency beat comes from the interplay between the Floquet frequency ω_{F}, present in eq 4, and the discrete nature of the N variable, associated with the modulation frequency Ω: the first one determines the oscillations of the reflectivity and the second one determines the sampling of the latter. It is precisely this mismatch between ω_{F} and Ω that results in these modulated oscillations in the classical reflectivity and, thus, in the average photon number. It is also clear from Figure 3c that the mean photon number in the second band is almost 1 order of magnitude smaller than in the fundamental one due to its strong dispersion. Additionally, the maximum value taken by the average photon number increases as we get closer to the bandgap, as seen in Figure 3d. The latter can be seen explicitly from eq 4: the maximum value taken by the classical reflectivity is $\mathcal{R}_{\max} = |(\boldsymbol{T})_{12}|^2/\sin^2(\omega_{\text{F}}T)$, which diverges whenever $\omega_{\text{F}}T \to n\pi$, which is the case at the band edges. Moreover, when $\omega_{\text{F}} = n\pi/T$, the mismatch between the Floquet frequency and the modulation one disappears and so does the frequency beat. Hence, for those modes within the bands, the closer to the band edges, the larger the number of photon pairs created and the weaker the frequency beat since constructive interference begins to build up (see SI for a more detailed discussion). Lastly, $\langle \hat{n}_k^{(N)} \rangle_{\text{vac}}$ vanishes identically for all values of N for $ck/\Omega = 0.5$ and 1. These values correspond to $(\boldsymbol{T})_{12} = 0$, in which the period of the oscillations in the mean photon number matches $2\pi/\Omega$, which is the period of the time modulation.

■ CONCLUSIONS

We have introduced a theory of photon pair creation in photonic time crystals and unveiled the connection between their classical electrodynamical properties, through their reflectivity, and quantum vacuum amplification processes by means of the squeezing parameter. Temporal interfaces result in dynamical Casimir processes, whereby pairs of forward and backward propagating photons are created from the quantum vacuum in a squeezed state, owing to momentum conservation. Critically, our approach provides a quantum treatment of the PTC regime within a Hermitian framework that is fully analytic, allowing us to fully treat modes within the momentum bandgaps. We also demonstrate that for the case of vacuum quantum amplification the average photon number coincides with the classical reflectivity of the photonic time crystal. Furthermore, we show that within the momentum bandgaps, the mean number of photons extracted from the vacuum grows exponentially with the number of periods N, while for band modes, it oscillates with a frequency beat and remains bounded. Moreover, since the formulas we have used apply to any periodic modulation, the phenomenology herein described will too be observed beyond the step case. Also, a step constitutes the building block for smoother variations, and it can be replicated with a $\tanh(t/\tau)$ profile for $\tau \lesssim T/10$, where $T = 2\pi/ck$.[45] Lastly, even though we have consider the case of a homogeneous system, classical and quantum amplification of waves would also be observed for a finite size system, as seen in refs 27, 65, and 66. Understanding quantum vacuum amplification in time varying media is important both from a fundamental perspective[46] and for its practical implications in the generation of quantum light sources.[42,67−69]

https://doi.org/10.1021/acsphotonics.4c02293
ACS Photonics 2025, 12, 1873−1880

ASSOCIATED CONTENT

Supporting Information

The Supporting Information is available free of charge at https://pubs.acs.org/doi/10.1021/acsphotonics.4c02293.

Detailed derivations of all the analytical formulas presented in the manuscript; Additionally, the generation of photon pairs for an expansion of the electromagnetic field in standing waves is discussed and compared with the plane-wave case found in the manuscript; Finally, the photon number statistics and the coherence of the quantum fields are studied in depth (PDF)

AUTHOR INFORMATION

Corresponding Authors

Jaime E. Sustaeta-Osuna − *Departamento de Física Teórica de la Materia Condensada, Universidad Autónoma de Madrid, E-28049 Madrid, Spain; Condensed Matter Physics Center (IFIMAC), Universidad Autónoma de Madrid, E-28049 Madrid, Spain*; Email: jaime.echave-sustaeta@uam.es

P. A. Huidobro − *Departamento de Física Teórica de la Materia Condensada, Universidad Autónoma de Madrid, E-28049 Madrid, Spain; Condensed Matter Physics Center (IFIMAC), Universidad Autónoma de Madrid, E-28049 Madrid, Spain; Instituto de Telecomunicações, Instituto Superior Tecnico-University of Lisbon, Lisboa 1049-001, Portugal*; orcid.org/0000-0002-7968-5158; Email: p.arroyo-huidobro@uam.es

Author

Francisco J. García-Vidal − *Departamento de Física Teórica de la Materia Condensada, Universidad Autónoma de Madrid, E-28049 Madrid, Spain; Condensed Matter Physics Center (IFIMAC), Universidad Autónoma de Madrid, E-28049 Madrid, Spain*; orcid.org/0000-0003-4354-0982

Complete contact information is available at: https://pubs.acs.org/10.1021/acsphotonics.4c02293

Notes

The authors declare no competing financial interest.

ACKNOWLEDGMENTS

The authors acknowledge fruitful conversations with J. B. Pendry, C. Sánchez-Muñoz, E. del Valle, and F. Laussy. We acknowledge funding from the Spanish Ministry for Science and Innovation (Grant No. RYC2021-031568-I and Project No. PID2022-141036NA-I00, financed by MCIN/AEI/10.13039/501100011033 and FSE+) and the CAM Consejería de Educación, Ciencia y Universidades, Viceconsejería de Universidades, Investigación y Ciencia, Dirección General de Investigación e Innovación Tecnológica (Sinergystic Project CAM 2020 NanoQuCo-CM ref. Y2020/TCS-6545 and CAM FPI Grant Ref. A281). P.A.H. further acknowledges funding from Fundaçao para a Cîencia e a Tecnologia under Project 2022.06797.PTDC.

REFERENCES

(1) Galiffi, E.; Tirole, R.; Yin, S.; Li, H.; Vezzoli, S.; Huidobro, P. A.; Silveirinha, M. G.; Sapienza, R.; Alù, A.; Pendry, J. B. Photonics of time-varying media. *Advanced Photonics* **2022**, *4*, 014002−014002.

(2) Pacheco-Peña, V.; Solís, D. M.; Engheta, N. Time-varying electromagnetic media: opinion. *Optical Materials Express* **2022**, *12*, 3829−3836.

(3) Engheta, N. Four-dimensional optics using time-varying metamaterials. *Science* **2023**, *379*, 1190−1191.

(4) Boltasseva, A.; Shalaev, V.; Segev, M. Photonic time crystals: from fundamental insights to novel applications: opinion. *Optical Materials Express* **2024**, *14*, 592−597.

(5) Moussa, H.; Xu, G.; Yin, S.; Galiffi, E.; Ra'di, Y.; Alù, A. Observation of temporal reflection and broadband frequency translation at photonic time interfaces. *Nat. Phys.* **2023**, *19*, 863−868.

(6) Zhou, Y.; Alam, M. Z.; Karimi, M.; Upham, J.; Reshef, O.; Liu, C.; Willner, A. E.; Boyd, R. W. Broadband frequency translation through time refraction in an epsilon-near-zero material. *Nat. Commun.* **2020**, *11*, 2180.

(7) Solís, D. M.; Kastner, R.; Engheta, N. Time-varying materials in the presence of dispersion: plane-wave propagation in a Lorentzian medium with temporal discontinuity. *Photonics Research* **2021**, *9*, 1842−1853.

(8) Pang, K.; Alam, M. Z.; Zhou, Y.; Liu, C.; Reshef, O.; Manukyan, K.; Voegtle, M.; Pennathur, A.; Tseng, C.; Su, X.; et al. Adiabatic frequency conversion using a time-varying epsilon-near-zero metasurface. *Nano Lett.* **2021**, *21*, 5907−5913.

(9) Liu, C.; Alam, M. Z.; Pang, K.; Manukyan, K.; Reshef, O.; Zhou, Y.; Choudhary, S.; Patrow, J.; Pennathurs, A.; Song, H.; et al. Photon acceleration using a time-varying epsilon-near-zero metasurface. *ACS Photonics* **2021**, *8*, 716−720.

(10) Tirole, R.; Vezzoli, S.; Galiffi, E.; Robertson, I.; Maurice, D.; Tilmann, B.; Maier, S. A.; Pendry, J. B.; Sapienza, R. Double-slit time diffraction at optical frequencies. *Nat. Phys.* **2023**, *19*, 999−1002.

(11) Huidobro, P. A.; Galiffi, E.; Guenneau, S.; Craster, R. V.; Pendry, J. B. Fresnel drag in space-time-modulated metamaterials. *Proc. Natl. Acad. Sci. U. S. A.* **2019**, *116*, 24943−24948.

(12) Wang, X.; Diaz-Rubio, A.; Li, H.; Tretyakov, S. A.; Alu, A. Theory and design of multifunctional space-time metasurfaces. *Physical Review Applied* **2020**, *13*, 044040.

(13) Li, H.; Yin, S.; He, H.; Xu, J.; Alù, A.; Shapiro, B. Stationary charge radiation in anisotropic photonic time crystals. *Phys. Rev. Lett.* **2023**, *130*, 093803.

(14) Chamanara, N.; Vahabzadeh, Y.; Caloz, C. Simultaneous control of the spatial and temporal spectra of light with space-time varying metasurfaces. *IEEE Transactions on Antennas and Propagation* **2019**, *67*, 2430−2441.

(15) Galiffi, E.; Xu, G.; Yin, S.; Moussa, H.; Ra'di, Y.; Alù, A. Broadband coherent wave control through photonic collisions at time interfaces. *Nat. Phys.* **2023**, *19*, 1703−1708.

(16) Prudêncio, F. R.; Silveirinha, M. G. Replicating physical motion with Minkowskian isorefractive spacetime crystals. *Nanophotonics* **2023**, *12*, 3007−3017.

(17) Prudêncio, F. R.; Silveirinha, M. G. Synthetic Axion Response with Space-Time Crystals. *Phys. Rev. Appl.* **2023**, *19*, 024031.

(18) Pendry, J.; Galiffi, E.; Huidobro, P. Photon conservation in trans-luminal metamaterials. *Optica* **2022**, *9*, 724−730.

(19) Bahrami, A.; Deck-Léger, Z.-L.; Caloz, C. Electrodynamics of accelerated-modulation space-time metamaterials. *Physical Review Applied* **2023**, *19*, 054044.

(20) Horsley, S. A.; Pendry, J. B. Quantum electrodynamics of time-varying gratings. *Proc. Natl. Acad. Sci. U. S. A.* **2023**, *120*, e2302652120.

(21) Morgenthaler, F. R. Velocity modulation of electromagnetic waves. *IRE Transactions on microwave theory and techniques* **1958**, *6*, 167−172.

(22) Felsen, L.; Whitman, G. Wave propagation in time-varying media. *IEEE Transactions on Antennas and Propagation* **1970**, *18*, 242−253.

(23) Fante, R. Transmission of electromagnetic waves into time-varying media. *IEEE Transactions on Antennas and Propagation* **1971**, *19*, 417−424.

https://doi.org/10.1021/acsphotonics.4c02293
ACS Photonics 2025, 12, 1873−1880

(24) Ramaccia, D.; Toscano, A.; Bilotti, F. Light propagation through metamaterial temporal slabs: reflection, refraction, and special cases. *Opt. Lett.* **2020**, *45*, 5836−5839.
(25) Ramaccia, D.; Alù, A.; Toscano, A.; Bilotti, F. Temporal multilayer structures for designing higher-order transfer functions using time-varying metamaterials. *Appl. Phys. Lett.* **2021**, *118*, na.
(26) Mirmoosa, M.; Mostafa, M.; Norrman, A.; Tretyakov, S. Time interfaces in bianisotropic media. *Physical Review Research* **2024**, *6*, 013334.
(27) Martínez-Romero, J. S.; Halevi, P. Parametric resonances in a temporal photonic crystal slab. *Phys. Rev. A* **2018**, *98*, 053852.
(28) Apffel, B.; Fort, E. Frequency conversion cascade by crossing multiple space and time interfaces. *Phys. Rev. Lett.* **2022**, *128*, 064501.
(29) Bacot, V.; Labousse, M.; Eddi, A.; Fink, M.; Fort, E. Time reversal and holography with spacetime transformations. *Nat. Phys.* **2016**, *12*, 972−977.
(30) Fink, M.; Fort, E. From the time-reversal mirror to the instantaneous time mirror. *European Physical Journal Special Topics* **2017**, *226*, 1477−1486.
(31) Reyes-Ayona, J.; Halevi, P. Observation of genuine wave vector (k or β) gap in a dynamic transmission line and temporal photonic crystals. *Appl. Phys. Lett.* **2015**, *107*, na.
(32) Wang, X.; Mirmoosa, M. S.; Asadchy, V. S.; Rockstuhl, C.; Fan, S.; Tretyakov, S. A. Metasurface-based realization of photonic time crystals. *Science Advances* **2023**, *9*, eadg7541.
(33) Liberal, I.; Engheta, N. Near-zero refractive index photonics. *Nat. Photonics* **2017**, *11*, 149−158.
(34) Reshef, O.; Giese, E.; Zahirul Alam, M.; De Leon, I.; Upham, J.; Boyd, R. W. Beyond the perturbative description of the nonlinear optical response of low-index materials. *Optics letters* **2017**, *42*, 3225−3228.
(35) Reshef, O.; De Leon, I.; Alam, M. Z.; Boyd, R. W. Nonlinear optical effects in epsilon-near-zero media. *Nature Reviews Materials* **2019**, *4*, 535−551.
(36) Bohn, J.; Luk, T. S.; Tollerton, C.; Hutchings, S. W.; Brener, I.; Horsley, S.; Barnes, W. L.; Hendry, E. All-optical switching of an epsilon-near-zero plasmon resonance in indium tin oxide. *Nat. Commun.* **2021**, *12*, 1017.
(37) Vezzoli, S.; Bruno, V.; DeVault, C.; Roger, T.; Shalaev, V. M.; Boltasseva, A.; Ferrera, M.; Clerici, M.; Dubietis, A.; Faccio, D. Optical time reversal from time-dependent epsilon-near-zero media. *Physical review letters* **2018**, *120*, 043902.
(38) Tirole, R.; Galiffi, E.; Dranczewski, J.; Attavar, T.; Tilmann, B.; Wang, Y.-T.; Huidobro, P. A.; Alú, A.; Pendry, J. B.; Maier, S. A.; et al. Saturable time-varying mirror based on an epsilon-near-zero material. *Physical Review Applied* **2022**, *18*, 054067.
(39) Lustig, E.; Segal, O.; Saha, S.; Bordo, E.; Chowdhury, S. N.; Sharabi, Y.; Fleischer, A.; Boltasseva, A.; Cohen, O.; Shalaev, V. M.; et al. Time-refraction optics with single cycle modulation. *Nanophotonics* **2023**, *12*, 2221−2230.
(40) Mendonça, J.; Guerreiro, A.; Martins, A. M. Quantum theory of time refraction. *Phys. Rev. A* **2000**, *62*, 033805.
(41) Mendonça, J.; Martins, A.; Guerreiro, A. Temporal beam splitter and temporal interference. *Phys. Rev. A* **2003**, *68*, 043801.
(42) Lyubarov, M.; Lumer, Y.; Dikopoltsev, A.; Lustig, E.; Sharabi, Y.; Segev, M. Amplified emission and lasing in photonic time crystals. *Science* **2022**, *377*, 425−428.
(43) Vázquez-Lozano, J. E.; Liberal, I. Shaping the quantum vacuum with anisotropic temporal boundaries. *Nanophotonics* **2023**, *12*, 539−548.
(44) Liberal, I.; Vázquez-Lozano, J. E.; Pacheco-Peña, V. Quantum antireflection temporal coatings: quantum state frequency shifting and inhibited thermal noise amplification. *Laser & Photonics Reviews* **2023**, *17*, 2200720.
(45) Ganfornina-Andrades, A.; Vázquez-Lozano, J. E.; Liberal, I. Quantum vacuum amplification in time-varying media with arbitrary temporal profiles. *Physical Review Research* **2024**, *6*, 043320.
(46) Nation, P.; Johansson, J.; Blencowe, M.; Nori, F. Colloquium: Stimulating uncertainty: Amplifying the quantum vacuum with superconducting circuits. *Rev. Mod. Phys.* **2012**, *84*, 1.
(47) Wilson, C. M.; Johansson, G.; Pourkabirian, A.; Simoen, M.; Johansson, J. R.; Duty, T.; Nori, F.; Delsing, P. Observation of the dynamical Casimir effect in a superconducting circuit. *nature* **2011**, *479*, 376−379.
(48) Lähteenmäki, P.; Paraoanu, G.; Hassel, J.; Hakonen, P. J. Dynamical Casimir effect in a Josephson metamaterial. *Proc. Natl. Acad. Sci. U. S. A.* **2013**, *110*, 4234−4238.
(49) Dodonov, V. Fifty years of the dynamical Casimir effect. *Physics* **2020**, *2*, 67−104.
(50) Pacheco-Peña, V.; Engheta, N. Antireflection temporal coatings. *Optica* **2020**, *7*, 323−331.
(51) Cassedy, E. S.; Oliner, A. A. Dispersion relations in time-space periodic media: Part I—Stable interactions. *Proceedings of the IEEE* **1963**, *51*, 1342−1359.
(52) Cassedy, E. S. Dispersion relations in time-space periodic media part II—Unstable interactions. *Proceedings of the IEEE* **1967**, *55*, 1154−1168.
(53) Pendry, J. Photon number conservation in time dependent systems. *Opt. Express* **2023**, *31*, 452−458.
(54) Park, J.; Kyungmin, L.; Zhang, R.-Y. Spontaneous Emission Decay and Excitation in Photonic Temporal Crystals. *arXiv:2404.13287 [physics.optics]* **2024**, na.
(55) Ashida, Y.; Gong, Z.; Ueda, M. Non-hermitian physics. *Adv. Phys.* **2020**, *69*, 249−435.
(56) Khurgin, J. B. Photonic time crystals and parametric amplification: similarity and distinction. *ACS Photonics* **2024**, *11*, 2150−2159.
(57) Barnett, S.; Radmore, P. M. *Methods in Theoretical Quantum Optics*; Oxford University Press, 2002; Vol. *15*.
(58) Milburn, G. Quantum optics. *Springer Handbook of Lasers and Optics* **2012**, 1305−1333.
(59) Gerry, C. C.; Knight, P. L. *Introductory Quantum Optics*; Cambridge University Press, 2023.
(60) Boyd, R. W.; Gaeta, A. L.; Giese, E. *Springer Handbook of Atomic, Molecular, and Optical Physics*; Springer, 2008; pp 1097−1110.
(61) Drummond, P. D.; Hillery, M. *The Quantum Theory of Nonlinear Optics*; Cambridge University Press, 2014.
(62) Glauber, R. J. The quantum theory of optical coherence. *Phys. Rev.* **1963**, *130*, 2529.
(63) Kim, M.; De Oliveira, F.; Knight, P. Properties of squeezed number states and squeezed thermal states. *Phys. Rev. A* **1989**, *40*, 2494.
(64) Mirmoosa, M.; Setälä, T.; Norrman, A. Quantum state engineering and photon statistics at electromagnetic time interfaces. *Physical Review Research* **2025**, *7*, 013120.
(65) Galiffi, E.; Wang, Y.-T.; Lim, Z.; Pendry, J. B.; Alù, A.; Huidobro, P. A. Wood anomalies and surface-wave excitation with a time grating. *Phys. Rev. Lett.* **2020**, *125*, 127403.
(66) Oue, D.; Ding, K.; Pendry, J. Noncontact frictional force between surfaces by peristaltic permittivity modulation. *Phys. Rev. A* **2023**, *107*, 063501.
(67) Sloan, J.; Rivera, N.; Joannopoulos, J. D.; Soljačić, M. Casimir light in dispersive nanophotonics. *Phys. Rev. Lett.* **2021**, *127*, 053603.
(68) Dikopoltsev, A.; Sharabi, Y.; Lyubarov, M.; Lumer, Y.; Tsesses, S.; Lustig, E.; Kaminer, I.; Segev, M. Light emission by free electrons in photonic time-crystals. *Proc. Natl. Acad. Sci. U. S. A.* **2022**, *119*, e2119705119.
(69) Bugler-Lamb, S.; Horsley, S. Polariton excitation rates from time dependent dielectrics. *Journal of Physics B: Atomic, Molecular and Optical Physics* **2016**, *49*, 235502.

https://doi.org/10.1021/acsphotonics.4c02293
ACS Photonics 2025, 12, 1873−1880